

Cite this: *J. Mater. Chem. C*, 2017,
5, 582

The effect of hexyl side chains on molecular conformations, crystal packing, and charge transport of oligothiophenes†

Benjamin P. Cherniawski,^a Steven A. Lopez,^b Edmund K. Burnett,^a Ilhan Yavuz,^b Lei Zhang,^a Sean R. Parkin,^c Kendall N. Houk^b and Alejandro L. Briseno^{*a}

We report substituent effects on conformational preferences and hole mobilities of 2,5-bis-(thiophen-2-yl)-thieno[3,2-*b*]thiophenes (BT TT) monomer and dimer, and hexyl derivatives. We employ single-crystal X-ray diffraction, quantum mechanical calculations, and thin-film transistors to explore the difference between monomer, dimer, and effect of hexyl substitution. The hexyl-substituted molecules show marked differences in solid-state packing compared to the unsubstituted analogs. Most notably, the alkylated monomer crystal structure exhibits terminal thiophenes in the *syn* conformation. In contrast, the unsubstituted monomer adopts the more common *anti* conformation. The hexyl-substituted dimer, however, features a mixture of *syn* and *anti* thiophenes. Gas phase conformations of oligomers rationalize the intrinsic conformational preferences. We use a multimode simulation to compute hole mobilities and find excellent agreement with experiment. Theoretical results support our hypothesis that alkyl side chains cause these small molecules to adopt orientations that enhance hole mobilities by an order of magnitude upon hexyl substitution of the monomer.

Received 25th October 2016,
Accepted 22nd November 2016

DOI: 10.1039/c6tc04612f

www.rsc.org/MaterialsC

Introduction

The polythiophene family (*e.g.* P3HT,¹ PBTTT,^{2,3} PQT⁴) are benchmark organic semiconductor polymers and provide a powerful platform for exploration of structure–property relations. In functional devices these materials show that control of microstructure is directly correlated to performance.^{5–13} Various additives (*i.e.*, nucleating agents and co-solvents) and processing techniques (*i.e.*, solvent annealing and shear/dip coating) have been explored to control critical morphologic parameters. Still, the molecular structure is the most fundamental factor controlling morphology.^{14,15} In this vein, we have performed a detailed study of structure–property relations in the oligo-BTTT system to provide insight on the effects of a major structural component to these systems, side chains.

Oligomers provide monodisperse, crystalline model systems that can aid in understanding of their parent polymers and their charge transport properties.^{4,5,16–27} These studies often leverage the crystal structures of the oligomers.^{4,5,16–23,28–46} We have identified a recurring theme in reported crystal structures: terminal thiophenes in many of these oligomer systems, oligo-QT⁴ and oligo-BTTT¹⁷ for examples, adopt *syn* (adjacent thiophene sulfurs on the same side) conformations. This is contrary to how these systems are typically depicted in the literature.

The majority of oligothiophene publications report interior alpha-coupled thiophenes as the expected *anti* (adjacent sulfurs on opposing sides) conformation in the single crystal.^{4,16,17,19,20,22,23,28,29,31,33–37,39–43,47–52} Exceptions exist, but typically are substituted with multiple chains, bulky groups, or flanked by relatively strongly interacting units.^{21,22,52} However, the terminal thiophene conformation is much less consistent and is undoubtedly influenced by substitution patterns and solid-state interactions. Many examples of terminal thiophenes in both *anti*^{4,16,17,19–22,28,29,33–35,37,39,41–43,47–52} and *syn*^{4,16,17,21–23,31,35,36,39,40,48,52} conformations exist in the literature.

In oligomer systems, the orientation preference in the crystal packing can be determined from crystal structure analysis. In order to better understand these conformational phenomena and the macroscopic effects, we characterized a series of substituted (C₆H₁₃) and unsubstituted PBTTT oligomers. Crystal structures

^a Department of Polymer Science and Engineering, Conte Research Center, University of Massachusetts, 120 Governors Drive, Amherst, MA, 01003, USA.
E-mail: abriseno@mail.pse.umass.edu

^b Department of Chemistry and Biochemistry, University of California Los Angeles, 607 Charles E. Young Drive, Los Angeles, CA 90095, USA

^c Department of Chemistry, University of Kentucky Lexington, Kentucky 40506-005, USA

† Electronic supplementary information (ESI) available: Detailed synthetic procedures. Characterization by ¹H NMR, MALDI-TOF, cyclic voltammograms, and opto-electronic data. The coordinates and energies for all BTTT oligomers. CCDC 1496597–1496599. For ESI and crystallographic data in CIF or other electronic format see DOI: 10.1039/c6tc04612f

were compared to gas-phase DFT calculations, and we computed torsional potentials to map conformational preferences. Finally, we measured and simulated charge transport for these molecules to understand the origin of the increased thin-film hole mobilities for alkyl-substituted PBTBT monomers.

Results and discussion

Crystal packing

The unsubstituted monomer (**1-H**) crystallizes with the triclinic $P\bar{1}$ space group with two crystallographically distinct half molecules in the asymmetric unit. It assumes the herringbone packing motif characterized by slipped edge-to-face interactions with an interplanar angle of 63° (Fig. 1a–c). Disorder within the unit cell could also be identified. The **1-H** has two major disorders: first the whole molecule is disordered by a $\sim 180^\circ$ rotation about the long molecular axis (still *anti-anti*, but rotated relative to the neighboring monomers). Secondly, the central thienothiophene unit can be flipped relative to one or both of the end thiophenes (*syn-anti* or *syn-syn*). Predominantly, the **1-H** molecule is *anti-anti* (adjacent sulfurs on opposing sides), though with a small population of *syn-syn* and/or *anti-syn* conformation. This indicates that *anti-anti* is the preferred conformation for **1-H**.

Despite many attempts, a **2-H** (structure in Fig. 2b) crystal suitable for X-ray analysis could not be obtained. We expect **2-H** to have many of the same features observed for **1-H** as well as a variety of other linear unsubstituted thiophene small molecules;

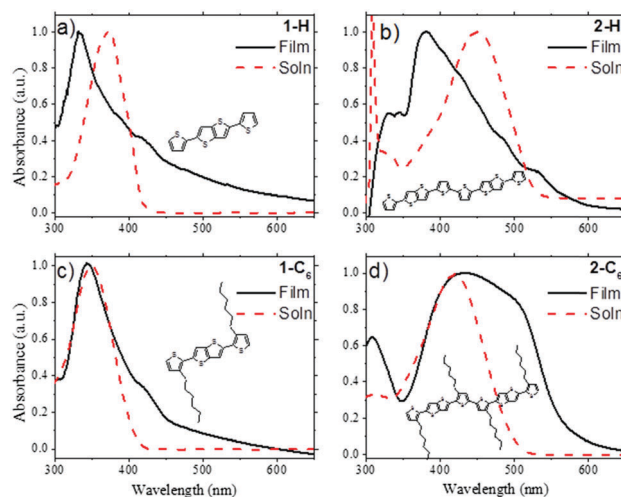


Fig. 2 Normalized UV-Vis spectra of the materials in chloroform [**2-H** in hot TCB] (dashed red) and thin film on glass (solid black): (a–d) **1-H**, **2-H**, **1-C₆**, **2-C₆**, respectively. Thin film of **2-H** was evaporated (~ 20 nm), all other films were spin coated from chloroform solution.

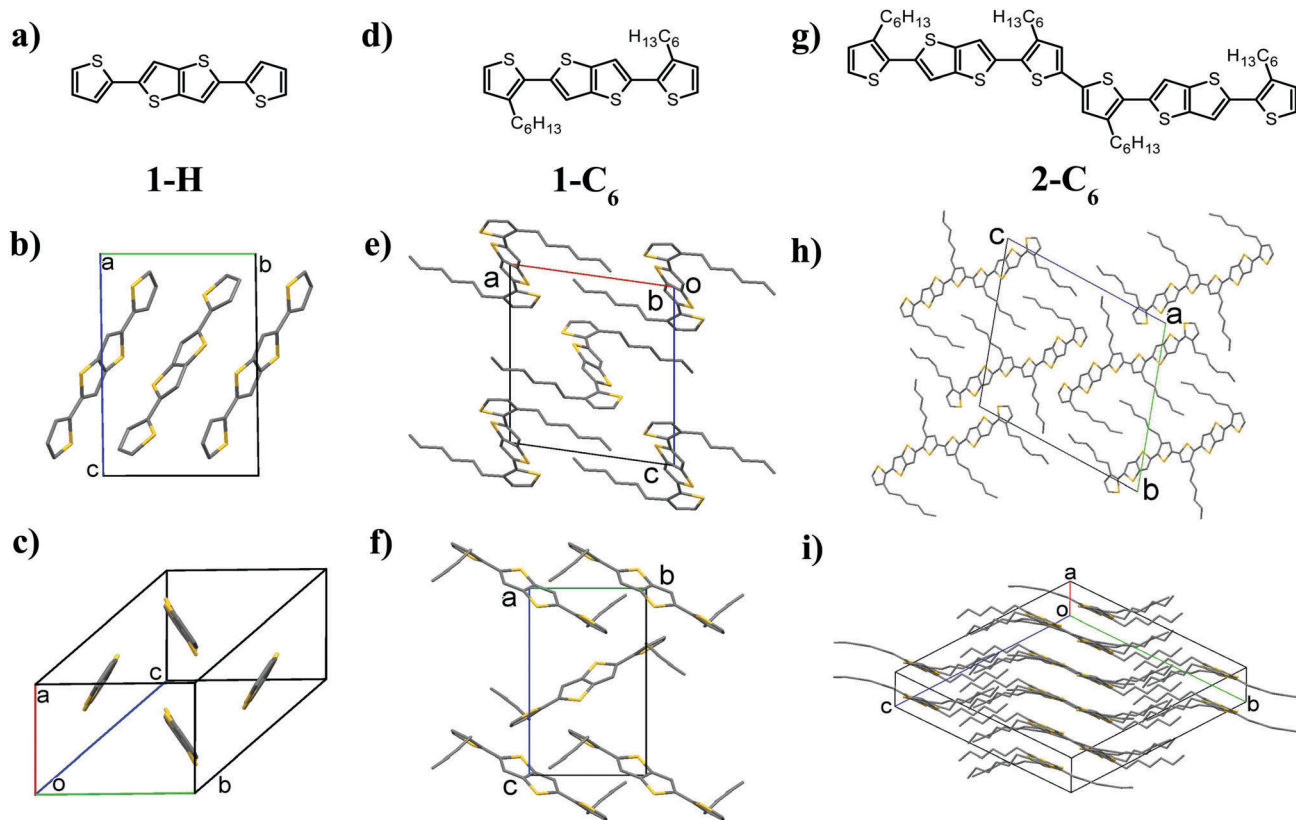


Fig. 1 Chemical structure and crystal packing of **1-H** (a–c), **1-C₆** (d–f), and **2-C₆** (g–i). (b) The **1-H** unit cell along the *a*-axis. (e and f) show the **1-C₆** unit cell along the *b*-axis and *a*-axis respectively. (h) The **2-C₆** unit cell along the *a*-axis. Hydrogens omitted for clarity. Crystals for X-ray analysis were grown by physical vapor transport (**1-H**) and by evaporation of solvent (**1-C₆** and **2-C₆**).

namely, a planar, all-*anti* conformation and herringbone packing motif.^{20,48,49}

The alkylated monomer (**1-C₆**) has space group $P2_1/n$, with a half molecule in the asymmetric unit and an end-to-face herringbone packing motif (Fig. 1d-f). The intermolecular backbone distance between adjacent molecules aligned along the *b*-axis do not indicate any close π - π interactions (>3.4 Å). Interestingly, the alkyl chains prevent rotational disorder of the terminal thiophene rings, but the central fused thienothiophene is disordered by a $\sim 180^\circ$ flip. The terminal thiophenes are predominantly in the *syn-syn* conformation (the preferred conformation), but with a large torsion angle of 38° with respect to the thienothiophene core.

The alkylated dimer (**2-C₆**) crystallizes in space group $P\bar{1}$ with one whole molecule in the asymmetric unit (Fig. 1g-i). The π - π distance in **2-C₆** is ~ 3.5 Å which also does not indicate significant π -interactions. This unusual packing has the hexyl chains curving away from a surprisingly planar backbone. The three hexyl groups on one side of the molecule interdigitate with hexyls on inversion-related molecules. The structure is severely disordered due to a complicated superposition of conformers. In brief, the disorder manifests from a 180° flip of one or both of the thienothiophenes. The thiophenes are again prevented from rotating due to alkylation, but experience small translational shifts depending on the adjacent thienothiophene conformation. Half of the molecule is predominantly *anti-anti* and the other half is 50/50 *anti-syn/syn-anti*. From what we observed in the hexyl-monomer preferences, the *anti* conformation is unexpected; we address this in the computational analysis section. The 50/50 occupancy of the other thienothiophene occurs because both conformations are essentially equivalent in energy (*anti-syn* = *syn-anti*).

Optical and electrochemical properties

The UV-Vis absorption spectra of the BTTT oligomers in chloroform solution (**2-H** in hot trichlorobenzene) and thin films are shown in Fig. 2. The solution maximum absorption of **1-H** shows a red shift compared to **1-C₆**; 373 and 350 nm respectively. The solid state for both monomers show a blue shift compared to their solution spectra, and the **1-H** shift is much larger than the **1-C₆** ($\Delta\lambda_{\text{max}} = 42$ nm and 8 nm respectively). The larger shift in the **1-H** λ_{max} is due to the H-aggregate arrangement in the solid state, as this phenomena is previously reported for this system.⁴⁶ The smaller blue shift of **1-C₆**, may be due to weaker H-aggregation, the loss in backbone planarity imposed by the molecular packing, or a combination of these effects.

The dimers (b and d) show a red-shifted absorption compared to the monomers due to the extended conjugation.⁵³ Among the dimers, **2-H** has a red shifted maximum absorption compared to the **2-C₆** due to its enhanced backbone planarity in solution. The solid state of **2-H** is also strongly blue shifted ($\Delta\lambda_{\text{max}} = 68$ nm) from its solution state spectra; likely due to H-aggregation. The **2-C₆** spectra shows a broadening and red-shift in the solid state. This lower energy absorption is evidence of a J-aggregate.⁴⁶

Computational analysis


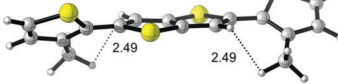
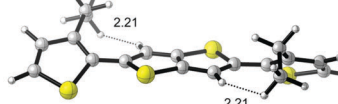
Gas-phase optimized structures were computed with the B97D density functional at the def2-TZV level of theory. Single-point energies were obtained from the optimized geometries with the B97D⁵⁴ functional and the large def2-QZVP basis set.⁵⁵ Following an experimental and theoretical approach previously used to understand the origin of paracrystalline disorder in PBTTT,⁵⁶ the hexyl group of **1-C₆** was replaced by methyl (**1-Me**) or ethyl (**1-Et**) groups to reduce computational expense.

In order to evaluate the steric effects, van der Waals radii⁵⁷ (r_{vdW}) [Sr_{vdW} : 1.8 Å, Hr_{vdW} : 1.2 Å] were used to identify critical interactions where interaction distances for atomic pairs is based on the sum of two r_{vdW} . S-S, H-H, and S-H interactions were evaluated for their influence on the final conformation when rotating the terminal ring. For the **1-H** system, only S-S interaction lengths were within the critical van der Waals distance. This suggests that $H_{\text{aryl}}-H_{\text{aryl}}$ interactions are negligible and S-S lone pair repulsion dominates the intrinsic preference for the *anti-anti* conformer of **1-H**.

Possible steric interactions were also evaluated for the **1-Me** and **1-Et** systems based on the r_{vdW} . The interaction distances for S- H_{alkyl} , $H_{\text{aryl}}-H_{\text{alkyl}}$, and S-S interaction were within the r_{vdW} sum. The $H_{\text{aryl}}-H_{\text{alkyl}}$ interaction is shown by the dotted lines in Table 1. For the alkylated systems, these additional interactions cause increased torsion in the optimized *syn-syn* conformation ($\sim 38^\circ$) vs. the **1-H** *syn-syn* local minima ($\sim 32^\circ$), and outweighs the S-S repulsion to prefer the *syn* conformer. The relative free energies of *syn* and *anti* conformations for the monomer systems are given in the ESI.†

We computed the torsional potential for **1-H** and **1-Me** to better understand how the unfavorable steric and orbital effects described above contribute to the overall torsional potentials about φ_1 and φ_2 (Fig. 3).⁵⁸ 0° indicates a planar *syn* conformation and 180° indicates a planar *anti* conformation. The rotations all exhibit maxima at $\pm 90^\circ$ and 0° , which are the rotational barriers. In the red line (circles), **1-H** shows a global minimum in the *anti-anti* conformation at approximately 180° . In the blue line (squares) with the conformers of **1-Me**, the lowest energy

Table 1 Optimized gas-phase geometries and dihedral angles for **1-H**, **1-Me** and **1-Et**. The dotted lines highlight important $H_{\text{aryl}}-H_{\text{alkyl}}$ interactions unsubstituted **1-H** monomer, **1-Me** and **1-Et** have global energy minima in the *syn-syn* conformation with relatively large torsion angles, 38° and 39° , respectively. These structures agree with the **1-C₆** crystal structure (38° torsion angle observed in crystal packing)

1-R	SCCS dihedral	Structure
1-H	168° [<i>anti-anti</i>]	
1-Me	38° [<i>syn-syn</i>]	
1-Et	39° [<i>syn-syn</i>]	

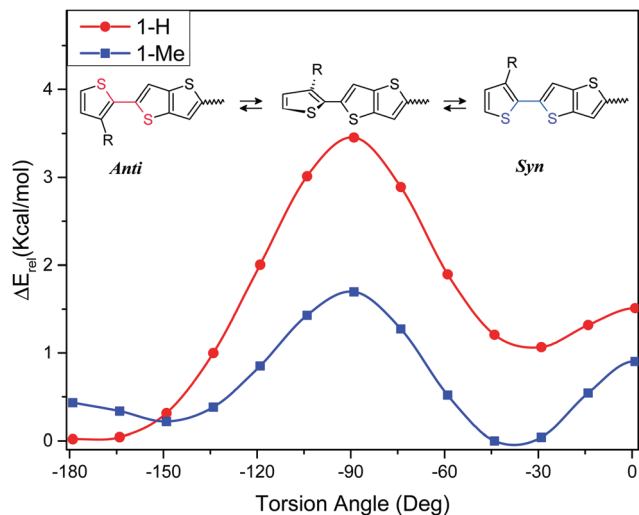


Fig. 3 Torsional potentials (kcal mol⁻¹) for SCCS torsion (in degrees) for **1-H** (red, circles) and **1-Me** (blue, squares). Computed using B97d/def2-QZVP//B97d/def2-TZV.

conformer is *syn-syn*, and S-S repulsion causes substantial deviation from planarity.

With a better understanding of the relative energies of intramolecular interactions we can now address the observed conformational preferences in the solid state. **1-H** prefers the planar, all-*anti* conformation because of S-S repulsion and planarizing contributions from π -electron delocalization. On the other hand, **1-C₆** intramolecular alkyl interactions outweigh the S-S repulsion and prompt this system to adopt the *syn-syn* conformation. In **2-C₆**, we can rationalize the presence of the *anti* conformation. The **1-Me** (open squares) in Fig. 3 best represents this interaction in the alkylated dimer. Although the global minimum is indeed a twisted *syn* conformation, the system is constrained to a planar conformation in the crystal.

Therefore, the thiophene–thienothiophene interactions can only adopt 0° or $\pm 180^\circ$. Comparing these two energies, the *anti* conformation is lower in energy and is thus favored.

It is important to note this single molecule, gas-phase analysis does not represent the vast parameter space and complexity of solid-state packing and intermolecular interactions. It can only serve as a starting point for analysis. This is especially evident in the **2-C₆** crystal packing where intermolecular dominates intramolecular interactions to planarize the repulsive S-S and S-H_{alkyl} interactions, and undoubtedly impacts the conformation of the terminal thiophenes to maximize backbone interactions and alkyl interdigitation.

Charge transport: experiment and simulation

We characterized charge transport in thin-film organic field-effect transistors (OFETs). Electrical measurements were performed under ambient conditions using a standard probe station. Thin-film OFETs were fabricated in a bottom-gate, bottom-contact geometry by spin coating 10 mg ml⁻¹ solution of oligothiophenes in chloroform at 3000 rpm for 60 s. The hole mobilities calculated in the saturated regime, threshold voltages, and current on/off ratios can be seen in Fig. 4. The measured mobilities of **1-H**, **1-C₆** and **2-C₆** are 3.2×10^{-4} , 5.2×10^{-3} , and 2.5×10^{-3} cm² V⁻¹ s⁻¹, respectively.

Both **1-C₆** and **2-C₆** have comparable mobilities in the thin film, however the **1-H** film is an order of magnitude lower than the alkylated oligomers. We performed charge transport simulations to understand the lower mobility of **1-H** compared to **1-C₆** and **2-C₆**.

We simulated the morphologies using classical molecular dynamics (MD) simulations (with AMBER⁵⁹) and charge-carrier dynamics using kinetic Monte Carlo⁶⁰ (kMC) simulations (using VOTCA⁶¹), based on Marcus theory.⁶² The multimode methodology was developed by Yavuz *et al.*, and has been used

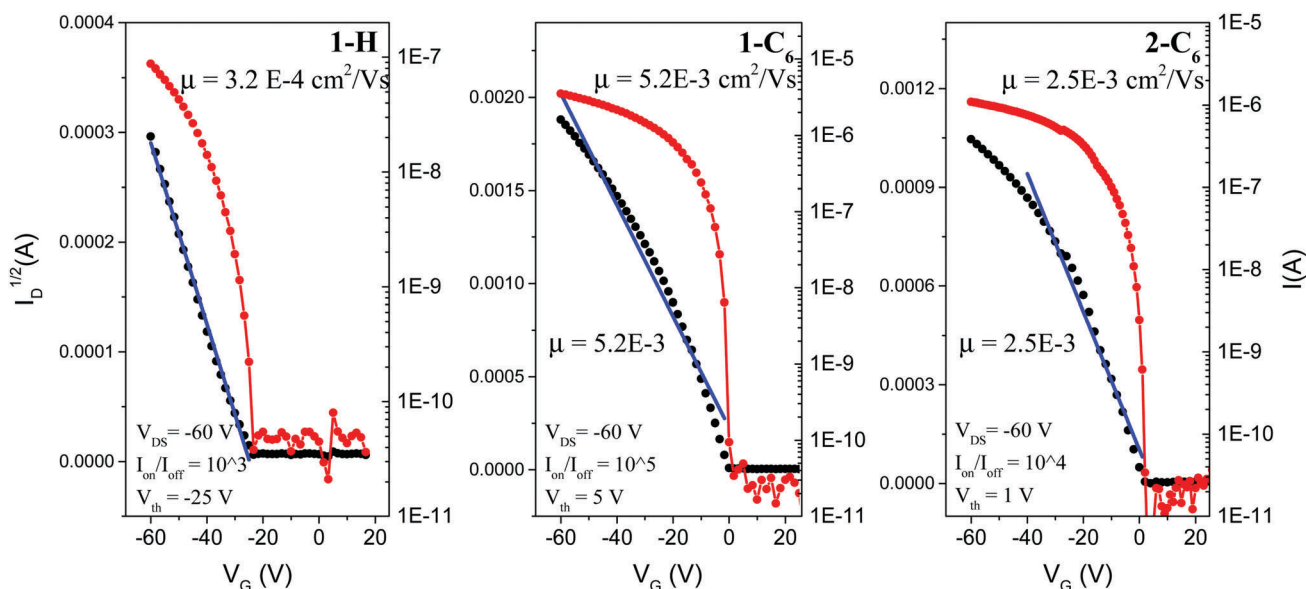


Fig. 4 The transfer characteristics of **1-H**, **1-C₆**, and **2-C₆** (left to right) BG-BC thin-film transistors.

to compute hole and electron mobilities.^{24–26} We calculated the charge-transport properties, reorganization energies (λ), energetic disorder (σ), electronic-coupling (J) distributions and the hole-mobilities (μ_{calc}) for these BTTT oligomers. The reorganization energies are calculated by the four-point rule⁶³ using the B3LYP⁶⁴ density functional using the 6-311G(d,p) basis set. The energetic disorder is obtained from the distribution of site-energy differences calculated by the Thole⁶⁵ model. The electronic-coupling between molecular dimers are calculated using Zerner's Intermediate Neglect of Differential Overlap.⁶⁶

The initial configurations were constructed as multiple copies of the unit cells in three crystallographic directions (Fig. 5). We used 1560, 1536 and 1536 molecules for **1-H**, **1-C₆**, and **2-C₆** respectively. The initial crystal models are equilibrated at 300 K in an *NPT* ensemble for 6 ns followed by a production run lasting 10 ns. The predicted morphologies are shown in Fig. 5 where the hexyl side chains are shown as green sticks for clarity. kMC simulations are performed on snapshots of the MD trajectories based on Marcus theory.

We sought to understand the origin of the mobilities by employing molecular dynamics simulations. Fig. 5 shows the initial configurations (left box) and the snapshots of representative disordered morphologies of **1-H**, **1-C₆**, and **2-C₆** materials (right box). Under each of these snapshots is the paracrystalline disorder parameter $\Delta g = \delta/\langle d \rangle$. Here, δ is the standard deviation and $\langle d \rangle$ is average of intermolecular distance distributions between oligomer centroids within the snapshot.

The **1-H** morphology is relatively unchanged after MD equilibration. However, **1-C₆** and **2-C₆** morphologies are after MD equilibration. These have paracrystallinity values of 1.4%, 1.8% and 2.7% respectively. The structural disorder leads to fluctuations in energetic landscapes during charge-transport, which enhances energetic disorder in these thin films. The energetic disorder parameter is predicted by computing the site energy differences. The site-energy difference is defined as the difference between HOMO energies of the system during charge-transfer. The distributions of site energies of the equilibrated morphologies are given in the ESI.† The energetic disorder is calculated from the standard deviations of these data distributions.

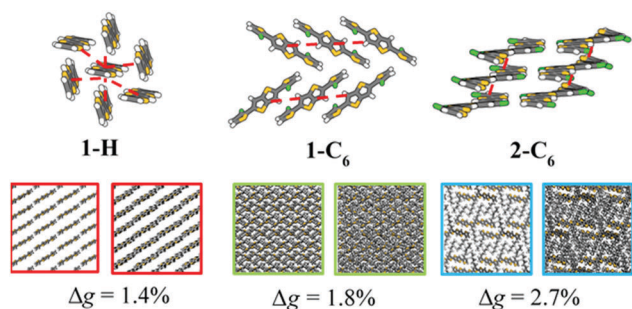


Fig. 5 (top row) Crystal structures of **1-H**, **1-C₆**, and **2-C₆** with principal charge transport direction indicated in red. Hexyl side-chains are represented with green sticks for clarity. (bottom row) Snapshot crystal configurations before (left) and after (right) introducing thermal disorder with AMBER molecular dynamics. **1-H** (red), **1-C₆** (green), **2-C₆** (blue) with the simulated paracrystalline disorder parameter, Δg .

Table 2 Reorganization energy (λ), energetic disorder (σ) ensemble-averaged electronic coupling of π - π stacking (J) experimental (μ_{exp}), and computed hole mobilities (μ_{calc}), for **1-H**, **1-C₆**, and **2-C₆**

1-R	λ (meV)	σ (meV)	J (meV)	μ_{calc} ($\text{cm}^2 \text{V}^{-1} \text{s}^{-1}$)	μ_{exp} ($\text{cm}^2 \text{V}^{-1} \text{s}^{-1}$)
1-H	420	80	6	2.3×10^{-4}	3.2×10^{-4}
1-C₆	618	56	170	1.0×10^{-3}	5.2×10^{-3}
2-C₆	638	54	104	6.3×10^{-3}	2.5×10^{-3}

The simulated mobilities (summarized in Table 2) are in good agreement of μ_{exp} ; these results predict the increased mobility for substituted BTTT systems (**1-C₆** and **2-C₆**). This is in line with our previous study where we established a methodology by which hole mobilities can be computed within an order of magnitude of the experimental mobility.²⁴ **1-H** features molecules arranged in a herringbone packing, while **1-C₆** and **2-C₆** monomers are slip-stacked. The herringbone packing minimizes orbital overlap (J); it is nearly two orders of magnitude lower than those of **1-C₆** and **2-C₆** (6 vs. 170 and 104 meV, respectively).

The alkyl chains stabilize the crystal packing due to favourable intermolecular dispersive interactions that result in slip-stacked arrangements for **1-C₆** and **2-C₆**. According to Marcus theory, hopping rate is proportional to J^2 , and the low J in **1-H** is responsible for the low mobility relative to **1-C₆** and **2-C₆**, despite the more favorable reorganization energy (420 vs. 618 and 638 meV, respectively).

Conclusions

We synthesized unsubstituted and hexyl-substituted monomers and dimers of the PBTTT system. These materials were characterized as single crystals and further evaluated with computational chemistry for insight into observed crystal-packing conformations and charge transport. **1-H** adopts the *anti-anti* conformation, while **1-C₆** adopts a *syn-syn* conformation. Computations reveal that destabilizing S-S closed-shell repulsions and alkyl chain steric repulsions are responsible for the *anti* conformational preference. The *syn-syn* conformation is preferred for **1-C₆** because repulsions between H_{alkyl} and S outweigh S-S or $\text{H}_{\text{alkyl}}\text{-H}_{\text{aryl}}$ repulsions. However, both of these factors contribute to the substantial backbone distortion (SCCS dihedral angle = 38°). The **2-C₆** single-crystal structure shows a nearly planar backbone with both *anti* and *syn* terminal thiophenes. While the *anti* conformation is preferred in a planar alkylated system, we attribute the presence *syn* terminal thiophene in the **2-C₆** to enhanced backbone interaction between adjacent molecules.

Charge-transport characteristics were determined by BGBC thin-film OFETs. We determined the hole mobilities for the **1-H**, **1-C₆** and **2-C₆** to be 3.4×10^{-4} , 5.2×10^{-3} , and 2.5×10^{-3} respectively. Computations of hole-mobilities for **1-H**, **1-C₆** and **2-C₆** reproduce the observed values within an order of magnitude.²⁴ They confirm that the alkyl chains result in enhanced charge-transport properties because of the slip-stacked arrangement

of **1-C₆** and **2-C₆**. The hole mobility of **1-H** is an order of magnitude lower because of substantially reduced electronic coupling in the herringbone arrangement.

Acknowledgements

B. P. C., E. K. B., L. Z., and A. L. B. acknowledge the National Science Foundation (DMR-1508627) and the Office of Naval Research (ONR N00014-16-1-2612). We are grateful to the DMREF program National Science Foundation (DMR-1335645) for financial support of this research. Computer resources also. Calculations were performed on the Hoffman2 cluster at UCLA and the Extreme Science and Engineering Discovery Environment (XSEDE), which is supported by the NSF (OCI-1053575). S. A. L. thanks the Department of Energy EERE Postdoctoral Fellowship for funding.

Notes and references

- 1 F. P. Koch, P. Smith and M. Heeney, *J. Am. Chem. Soc.*, 2013, **135**, 13695–13698.
- 2 I. McCulloch, M. Heeney, C. Bailey, K. Genevicius, I. MacDonald, M. Shkunov, D. Sparrowe, S. Tierney, R. Wagner and W. Zhang, *Nat. Mater.*, 2006, **5**, 328–333.
- 3 D. M. DeLongchamp, R. J. Kline, E. K. Lin, D. A. Fischer, L. J. Richter, L. A. Lucas, M. Heeney, I. McCulloch and J. E. Northrup, *Adv. Mater.*, 2007, **19**, 833–837.
- 4 L. Zhang, N. S. Colella, F. Liu, S. Trahan, J. K. Baral, H. H. Winter, S. C. Mannsfeld and A. L. Briseno, *J. Am. Chem. Soc.*, 2012, **135**, 844–854.
- 5 L. Zhang, N. S. Colella, B. P. Cherniawski, S. C. Mannsfeld and A. L. Briseno, *ACS Appl. Mater. Interfaces*, 2014, **6**, 5327–5343.
- 6 M. A. Baklar, F. Koch, A. Kumar, E. B. Domingo, M. Campoy-Quiles, K. Feldman, L. Yu, P. Wobkenberg, J. Ball and R. M. Wilson, *Adv. Mater.*, 2010, **22**, 3942–3947.
- 7 D. M. DeLongchamp, R. J. Kline, D. A. Fischer, L. J. Richter and M. F. Toney, *Adv. Mater.*, 2011, **23**, 319–337.
- 8 A. Salleo, R. J. Kline, D. M. DeLongchamp and M. L. Chabinyc, *Adv. Mater.*, 2010, **22**, 3812–3838.
- 9 H. Sirringhaus, *Adv. Mater.*, 2014, **26**, 1319–1335.
- 10 A. A. Virkar, S. Mannsfeld, Z. Bao and N. Stingelin, *Adv. Mater.*, 2010, **22**, 3857–3875.
- 11 M. Mas-Torrent and C. Rovira, *Chem. Rev.*, 2011, **111**, 4833–4856.
- 12 J. Rivnay, S. C. Mannsfeld, C. E. Miller, A. Salleo and M. F. Toney, *Chem. Rev.*, 2012, **112**, 5488–5519.
- 13 R. Noriega, J. Rivnay, K. Vandewal, F. P. Koch, N. Stingelin, P. Smith, M. F. Toney and A. Salleo, *Nat. Mater.*, 2013, **12**, 1038–1044.
- 14 P. M. Beaujuge and J. M. Fréchet, *J. Am. Chem. Soc.*, 2011, **133**, 20009–20029.
- 15 J. Mei, Y. Diao, A. L. Appleton, L. Fang and Z. Bao, *J. Am. Chem. Soc.*, 2013, **135**, 6724–6746.
- 16 C.-F. Huang, S.-L. Wu, Y.-F. Huang, Y.-C. Chen, S.-T. Chang, T.-Y. Wu, K.-Y. Wu, W.-T. Chuang and C.-L. Wang, *Chem. Mater.*, 2016, **28**, 5175–5190.
- 17 L. Zhang, F. Liu, Y. Diao, H. S. Marsh, N. S. Colella, A. Jayaraman, T. P. Russell, S. C. Mannsfeld and A. L. Briseno, *J. Am. Chem. Soc.*, 2014, **136**, 18120–18130.
- 18 S. S. Zade, N. Zamoshchik and M. Bendikov, *Acc. Chem. Res.*, 2010, **44**, 14–24.
- 19 C. Zhou, Y. Liang, F. Liu, C. Sun, X. Huang, Z. Xie, F. Huang, J. Roncali, T. P. Russell and Y. Cao, *Adv. Funct. Mater.*, 2014, **24**, 7538–7547.
- 20 L. Antolini, G. Horowitz, F. Kouki and F. Garnier, *Adv. Mater.*, 1998, **10**, 382–385.
- 21 A. Facchetti, M.-H. Yoon, C. L. Stern, G. R. Hutchison, M. A. Ratner and T. J. Marks, *J. Am. Chem. Soc.*, 2004, **126**, 13480–13501.
- 22 A. N. Sokolov, J. C. Sumrak and L. R. MacGillivray, *Chem. Commun.*, 2010, **46**, 82–84.
- 23 L. Wang, X. Zhang, J. Zhang, H. Tian, Y. Lu, Y. Geng and F. Wang, *J. Mater. Chem. C*, 2014, **2**, 9978–9986.
- 24 I. Yavuz, B. N. Martin, J. Park and K. Houk, *J. Am. Chem. Soc.*, 2015, **137**, 2856–2866.
- 25 I. Yavuz, S. A. Lopez, J. B. Lin and K. Houk, *J. Mater. Chem. C*, 2016, DOI: 10.1039/C6TC03823A.
- 26 I. Yavuz and S. A. Lopez, *Phys. Chem. Chem. Phys.*, 2016, DOI: 10.1039/c6cp06431k.
- 27 J. Roncali, P. Leriche and P. Blanchard, *Adv. Mater.*, 2014, **26**, 3821–3838.
- 28 L. Antolini, U. Folli, F. Goldoni, D. Iarossi, A. Mucci and L. Schenetti, *Acta Polym.*, 1996, **47**, 265–268.
- 29 M. M. Bader, P.-T. T. Pham and E. H. Elandaloussi, *Cryst. Growth Des.*, 2010, **10**, 5027–5030.
- 30 P. Bäuerle and J. Cremer, *Chem. Mater.*, 2008, **20**, 2696–2703.
- 31 P. A. Chaloner, S. R. Gunatunga and P. B. Hitchcock, *J. Chem. Soc., Perkin Trans. 2*, 1997, 1597–1604.
- 32 J. Chisaka, M. Lu, S. Nagamatsu, M. Chikamatsu, Y. Yoshida, M. Goto, R. Azumi, M. Yamashita and K. Yase, *Chem. Mater.*, 2007, **19**, 2694–2701.
- 33 J. T. Henssler and A. J. Matzger, *J. Org. Chem.*, 2012, **77**, 9298–9303.
- 34 S. Hotta and K. Waragai, *J. Mater. Chem.*, 1991, **1**, 835–842.
- 35 H. Inubushi, Y. Hattori, Y. Yamanoi and H. Nishihara, *J. Org. Chem.*, 2014, **79**, 2974–2979.
- 36 J. H. Liao, M. Benz, E. Legoff and M. G. Kanatzidis, *Adv. Mater.*, 1994, **6**, 135–138.
- 37 H. Mo, K. R. Radke, K. Ogawa, C. L. Heth, B. T. Erpelding and S. C. Rasmussen, *Phys. Chem. Chem. Phys.*, 2010, **12**, 14585–14595.
- 38 M. Moreno, M. Casalegno, G. Raos, S. V. Meille and R. Po, *J. Phys. Chem. B*, 2010, **114**, 1591–1602.
- 39 T. Otani, M. Hachiya, D. Hashizume, T. Matsuo and K. Tamao, *Chem. – Asian J.*, 2011, **6**, 350–354.
- 40 T. M. Pappenfus, D. K. Schneiderman, J. Casado, J. T. López Navarrete, M. C. Ruiz Delgado, G. Zotti, B. Vercelli, M. D. Lovander, L. M. Hinkle and J. N. Bohnsack, *Chem. Mater.*, 2010, **23**, 823–831.

- 41 C. Reese, M. E. Roberts, S. R. Parkin and Z. Bao, *Adv. Mater.*, 2009, **21**, 3678–3681.
- 42 Y. Shibata, T. Kono, N. Ohashi and Y. Yoshida, *Thin Solid Films*, 2015, **583**, 163–169.
- 43 W. Yue, H. Tian, N. Hu, Y. Geng and F. Wang, *Cryst. Growth Des.*, 2008, **8**, 2352–2358.
- 44 S. S. Zade and M. Bendikov, *Chem. – Asian J.*, 2007, **13**, 3688–3700.
- 45 G. Zhang, Y. Pei, J. Ma, K. Yin and C.-L. Chen, *J. Phys. Chem. B*, 2004, **108**, 6988–6995.
- 46 X. Zhang, J. P. Johnson, J. W. Kampf and A. J. Matzger, *Chem. Mater.*, 2006, **18**, 3470–3476.
- 47 G. Barbarella, M. Zambianchi, R. Di Toro, M. Colonna, L. Antolini and A. Bongini, *Adv. Mater.*, 1996, **8**, 327–331.
- 48 D. Fichou, *J. Mater. Chem.*, 2000, **10**, 571–588.
- 49 D. Fichou, B. Bachet, F. Demanze, I. Billy, G. Horowitz and F. Garnier, *Adv. Mater.*, 1996, **8**, 500–504.
- 50 R. Fitzner, E. Reinold, A. Mishra, E. Mena-Osteritz, H. Ziehlke, C. Körner, K. Leo, M. Riede, M. Weil, O. Tsaryova, A. Weiß, C. Urich, M. Pfeiffer and P. Bäuerle, *Adv. Funct. Mater.*, 2011, **21**, 897–910.
- 51 J. Luo, H. Qu, J. Yin, X. Zhang, K.-W. Huang and C. Chi, *J. Mater. Chem.*, 2009, **19**, 8202–8211.
- 52 L. Maini, F. Gallino, M. Zambianchi, M. Durso, M. Gazzano, K. Rubini, D. Gentili, I. Manet, M. Muccini and S. Toffanin, *Chem. Commun.*, 2015, **51**, 2033–2035.
- 53 H. Meier, U. Stalmach and H. Kolshorn, *Acta Polym.*, 1997, **48**, 379–384.
- 54 S. Grimme, *J. Comput. Chem.*, 2006, **27**, 1787–1799.
- 55 A. Schäfer, H. Horn and R. Ahlrichs, *J. Chem. Phys.*, 1992, **97**, 2571–2577.
- 56 Z. Fei, P. Pattanasattayavong, Y. Han, B. C. Schroeder, F. Yan, R. J. Kline, T. D. Anthopoulos and M. Heeney, *J. Am. Chem. Soc.*, 2014, **136**, 15154–15157.
- 57 A. Bondi, *J. Phys. Chem.*, 1964, **68**, 441–451.
- 58 N. E. Jackson, B. M. Savoie, K. L. Kohlstedt, M. Olvera De La Cruz, G. C. Schatz, L. X. Chen and M. A. Ratner, *J. Am. Chem. Soc.*, 2013, **135**, 10475–10483.
- 59 R. Salomon-Ferrer, A. W. Götz, D. Poole, S. Le Grand and R. C. Walker, *J. Chem. Theory Comput.*, 2013, **9**, 3878–3888.
- 60 V. Rühle, A. Lukyanov, F. May, M. Schrader, T. Vehoff, J. Kirkpatrick, B. R. Baumeier and D. Andrienko, *J. Chem. Theory Comput.*, 2011, **7**, 3335–3345.
- 61 V. Rühle, C. Junghans, A. Lukyanov, K. Kremer and D. Andrienko, *J. Chem. Theory Comput.*, 2009, **5**, 3211–3223.
- 62 R. A. Marcus, *J. Chem. Phys.*, 1956, **24**, 966–978.
- 63 B. Kippelen and J.-L. Brédas, *Energy Environ. Sci.*, 2009, **2**, 251–261.
- 64 A. D. Becke, *J. Chem. Phys.*, 1993, **98**, 5648–5652.
- 65 B. T. Thole, *Chem. Phys.*, 1981, **59**, 341–350.
- 66 J. Ridley and M. Zerner, *Theor. Chim. Acta*, 1973, **32**, 111–134.